Journal of Molecular Catalysis A: Chemical 353–354 (2012) 13–21

Contents lists available at SciVerse ScienceDirect

Journal of Molecular Catalysis A: Chemical

journal homepage: www.elsevier.com/locate/molcata

Acyl-substituted ferrocenes as driers for solvent-borne alkyd paints

Milan Erben[a,*], David Veselý[b], Jaromír Vinklárek[a], Jan Honzíček[a]

[a] Department of General and Inorganic Chemistry, Faculty of Chemical Technology, University of Pardubice, Studentská 573, 532 10 Pardubice, Czech Republic
[b] Institute of Chemistry and Technology of Macromolecular Materials, Faculty of Chemical Technology, University of Pardubice, Studentská 573, 532 10 Pardubice, Czech Republic

ARTICLE INFO

Article history:
Received 2 August 2011
Received in revised form 24 October 2011
Accepted 29 October 2011
Available online 20 November 2011

Keywords:
Ferrocenes
Alkyd
Drier
FTIR
ESR

ABSTRACT

Ferrocenes bearing acyl substituents in the cyclopentadienyl rings [Fe(η^5-C_5H_4COR)(η^5-C_5H_5)] and [Fe(η^5-$C_5H_4COR)_2$] (R = CH_3, CF_3 and Ph) were examined as new driers for solvent-borne alkyd binder. All studied ferrocenes were found to be active catalysts for cross-linking reaction of the alkyd. These iron(II) compounds give solid polymeric films with hardness and drying time comparable to the commercial cobalt(II) drier. Acetyl- and benzoyl-substituted ferrocenes show an excellent synergic effect with the cobalt drier giving hard polymeric films within short drying time. The kinetics of the alkyd autoxidation was followed by FTIR spectroscopy. Spin-trapping ESR technique has proven the important role of the ferrocenium cation upon decomposition of hydroperoxides by ferrocene-based driers. The peroxy and alkoxy radicals, appearing in drying process, were resolved by the new spin trap methyl-*N*-mesityl nitrone.

1. Introduction

Alkyd resins are polyesters modified with unsaturated fatty acids. They are used as general-purpose binders in modern coatings. Since the alkyds contain up to 70 wt.% of natural oils, these resins are important binder systems made from renewable resources [1,2]. The alkyd drying involves the oxidation of unsaturated chains that is generally slow process requiring catalysis with transition metal compounds [3]. The role of metal drier in the curing process has been extensively studied on model systems. It has been found that the most important function of the catalyst is the decomposition of relatively stable hydroperoxides into radicals. It is known as the Haber–Weiss mechanism [4–7]:

$$ROOH + M^{(n)+} \rightarrow RO^{\bullet} + M^{(n+1)+} + OH^{-}$$

$$ROOH + M^{(n+1)+} \rightarrow ROO^{\bullet} + M^{(n)+} + H^{+}$$

Currently, cobalt carboxylates such as cobalt(II) 2-ethylhexanoate (**Co Nuodex**) are the most powerful catalysts for drying of the alkyd resins [8]. However, the pronounced genotoxicity and carcinogenicity of cobalt(II) compounds stimulate the legislative pressure on the paint-producing industry to replace these compounds with less toxic metal driers such as manganese compounds [9–13].

Ferrocene [$FeCp_2$] (Cp = η^5-cyclopentadienyl) is stable 18-electron complex that could be easily oxidized to 17-electron ferrocenium cation $[FeCp_2]^+$. This one-electron redox system is fully reversible and ferrocene/ferrocenium couple is used as standard redox system in electrochemistry. Furthermore, the redox potential of this redox pair is tunable through the substitution in the cyclopentadienyl rings. These properties together with high thermodynamic stability (ferrocene is stable up to 400 °C), high solubility in common organic solvents, chemical inertness and low toxicity make from ferrocene an ideal electron carrier [14]. Ferrocene derivatives are currently studied as catalysts, in drug design, as building blocks in material engineering and in nanotechnology [15–18]. Reaction of ferrocene or ferrocene monocarboxylic acid with hydroperoxides has been successively used for amperometric determination of lipid hydroperoxides in natural materials. [19] In 2006, our group has established ferrocene as the co-drier for autoxidation of the alkyd resins [20]. Further investigation of the ring-substituted derivatives has shown that the compounds bearing electron-withdrawing substituents are significantly more active than unsubstituted ferrocene or methyl-substituted congeners [21–23].

The aim of this study is to describe the drying behavior of acyl-substituted ferrocenes [Fe(Cp)(η^5-$C_5H_4COCH_3$)] (**Ac_1Fc**), [Fe(Cp)(η^5-$C_5H_4COCF_3$)] (**Tfa_1Fc**), [Fe(Cp)(η^5-C_5H_4COPh)] (**Bz_1Fc**), [Fe(η^5-$C_5H_4COCH_3)_2$] (**Ac_2fc**), [Fe(η^5-$C_5H_4COCF_3)_2$] (**Tfa_2fc**), [Fe(η^5-$C_5H_4COPh)_2$] (**Bz_2fc**) and compare it with the commercial cobalt(II) paint drier (**Co Nuodex**) and unsubstituted ferrocene (**Fc**), respectively, see Scheme 1. The catalyzed autoxidation of the solvent-borne alkyd was examined by drying time and film hardness measurements. Kinetics of the alkyd drying was followed by time-resolved FTIR spectroscopy. The synergic effects between acylferocenes and **Co Nuodex** were also studied. The role of

* Corresponding author. Tel.: +420 46603 7163; fax: +420 46603 7068.
E-mail address: milan.erben@upce.cz (M. Erben).

1381-1169/$ – see front matter © 2011 Elsevier B.V. All rights reserved.
doi:10.1016/j.molcata.2011.10.024

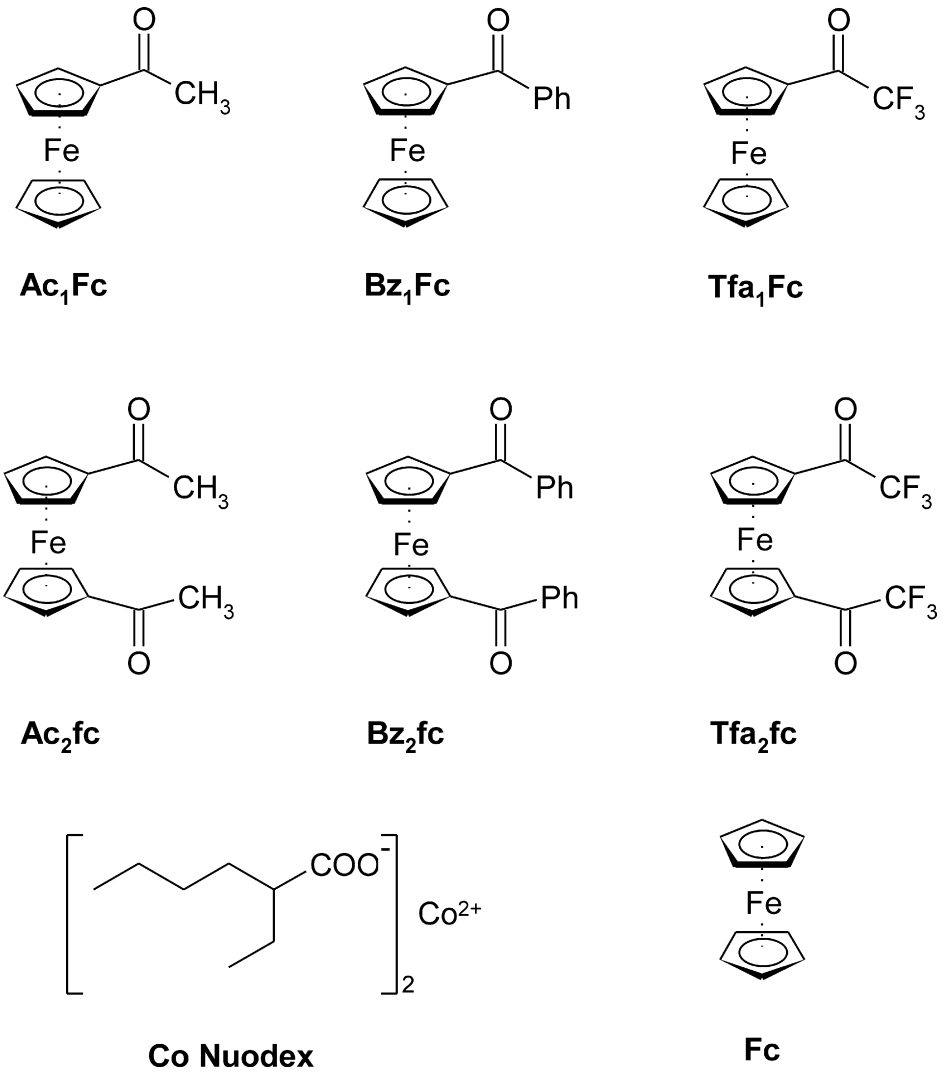

Scheme 1. Chemical structure of studied driers.

ferrocene drier in the mechanism of hydroperoxides decomposition was studied by ESR spectroscopy. The peroxy and alkoxy radicals, appearing upon drying process, were resolved by the new spin trap methyl-*N*-mesityl nitrone (MMN).

2. Experimental

2.1. Materials and methods

The compounds **Bz_1Fc**, **Bz_2fc**, **Ac_1Fc**, **Ac_2fc** and **Fc** were purchased from Sigma–Aldrich and used after vacuum sublimation. Organometallic salts $[FeCp_2]BF_4$ (**$FcBF_4$**) and $[FeCp(\eta^6$-toluene$)]PF_6$ were prepared following published procedures [24,25]. Spin trap MMN has been prepared by UV photolysis of nitromesitylene dissolved in triethylamine. Analytically pure MMN was obtained by column chromatography followed with twice crystallization from hexane [26]. Sodium salt $Na(C_5H_4COCF_3)$ has been synthesized by the reaction of sodium cyclopentadienide with CF_3COOCH_3 at −15 °C and isolated as yellow crystalline powder [27]. Preparation and purification of ferrocene derivatives has been carried out using standard Schlenk and vacuum technique, solvents were dried and deoxygenated with appropriate reagents (Na/K alloy, benzophenone ketylate, etc.) The commercial cobalt drier based on Co(II) 2-ethylhexanoate (**Co Nuodex**) was obtained from Borchers GmbH. The solvent-borne phthalic-type alkyd resin modified with tall oil (Balkyd T49 WX55, 55% of dry matter content in white spirit) supplied by Barvy a laky Hostivař a.s. has been used for both kinetic measurements and the determination of prepared films properties. Neutralization value of alkyd was 7 mg KOH per gram of resin. Technical ethyl linoleate (60%; remainder ethyl oleate, ethyl palmitate and ethyl stearate) was obtained from Sigma–Aldrich and used without further purification. Linoleic acid (60%, natural), linolenic acid (70%, natural) and methyl linolenate (65%, technical) were obtained from Acros Organic. The ^1H, ^{13}C and ^{19}F NMR spectra were measured at 300 K on a Bruker Avance500. The chemical shifts were referenced to external neat $(CH_3)_4Si$ or $CFCl_3$, respectively. IR spectra were recorded in the range of 4000–400 cm^{-1} on a Nicolet Magna 550 FTIR spectrometer in KBr pellets. Raman spectra were recorded in the range of 4000–50 cm^{-1} on a Bruker IFS 55 with FRA 106 extension. Electronic absorption spectra were run on a Hewlett-Packard 8453 spectrometer with diode array. Elemental analyses were done on a Fisions EA 1108 microanalyzer.

2.2. Time-resolved FTIR experiments

The oxidation of alkyd resin was followed by time-resolved FTIR on a Nicolet Magna 550 FTIR and on Nicolet 6700 spectrophotometers (32 scans per spectrum with a resolution of 2 cm^{-1}) in the

range of 4000–500 cm^{-1}. Mixture of alkyd resin with appropriate drier was spread on the NaCl plate using an applicator with slot width 0.1 mm. Sample was placed in the spectrometer and IR spectrum was recorded each 5 min at 23 °C. Collected IR spectra were integrated using fixed two-point baseline in the bounds 3650–3125 cm^{-1} (OH stretch), 3014–2997 cm^{-1} (methylenic CH stretch) and 1011–947 cm^{-1} (conjugated double bonds), respectively. The error in determination of k_{CH} was less than 10% (three independent measurements for each run).

2.3. ESR spectroscopy

The ESR spectra were measured in 50 μl quartz micropipettes (1 mm inner diameter) on a Miniscope MS300 X-band spectrometer. The ESR spectrometer settings for radical adducts were: microwave power 50 mW (16 mW for samples with cobalt drier); modulation amplitude 0.2 mT; time constant 0.5 s; B_0 field 335.1 mT, scan range 9.9 mT; scan time 360 s. Hyperfine splitting constants a_N and a_H were determined by computer simulations performed in PEST Winsim software downloaded from http://www.niehs.nih.gov/. The observed error in determination of a_N and a_H for spin-adducts was less than ±0.5% and ±1%, respectively.

The ESR spectra of PBN adduct shown in Fig. 6 (Section 3.5) correspond to samples with following composition. Sample **A**: 3.10^{-3} M **Bz_1Fc**, 1.10^{-3} M PBN, 0.15 M ^{t}BuOOH in toluene (spectrometer gain 800, three accumulated spectra); sample **B**: 2.10^{-3} M **$FcBF_4$** (dosed as 3 μl of 0.2 M solution in MeCN, gain 400), 1.10^{-3} M PBN, 0.15 M ^{t}BuOOH in toluene; sample **C**: 2.10^{-4} M **Co Nuodex**, 4.10^{-3} M PBN, 0.15 M ^{t}BuOOH in toluene (gain 200). The ESR spectra of MMN adducts shown in Fig. 7 (Section 3.5) correspond to samples with following composition. Sample **A**: 2.10^{-3} M **Bz_1Fc**, 4.10^{-3} MMN, 0.15 M ^{t}BuOOH in toluene (gain 800, three accumulated spectra); sample **B**: 2.10^{-3} M **$FcBF_4$** (dosed as 3 μl of 0.2 M solution in MeCN, gain 400), 4.10^{-3} M MMN, 0.15 M ^{t}BuOOH in toluene; sample **C**: 3.10^{-4} M **Co Nuodex**, 4.10^{-3} M MMN, 0.15 M ^{t}BuOOH in toluene (gain 200), sample **D**: identical to sample **C**, but after 120 min exposition to diffuse laboratory light.

2.4. Film drying time and hardness film determination

The drying performance of studied catalysts has been determined using a BYK Drying Time Recorder. The instrument is a straight-line recorder equipped with hemispherical ended needle (5 g weight used) that travel the length of the test strip under standard laboratory conditions (temperature 23 °C, relative air humidity 50%). A glass test strip was prepared by casting a film upon it (thickness was 38 μm of wet film). The trace left on the film during the drying has been used to define drying time as described previously [4].

Film hardness development was monitored using a Persoz-type pendulum (Elcometer Pendulum Hardness Tester, United Kingdom) in conformity with ISO 1522. The method is based on registering the number of pendulum swings it takes before the amplitude of the pendulum is damped to a certain extent. The more swings observed, the harder is the film. A plain glass test plate (10 cm × 20 cm) was coated with a 90 μm film (wet thickness) dried with the appropriate drier system and film hardness was measured within 100 days. The measured value was related to the hardness of a glass standard and expressed as relative hardness in percents. The error in determination of surface hardness was estimated to be ±0.5%. On summarizing of obtained data, dependence of film hardness versus time has been determined.

2.5. Preparation of [FeCp($C_5H_4COCF_3$)], Tfa_1Fc

1.074 g (3 mmol) [FeCp(η^6-toluene)]PF_6 was dissolved in 100 ml of acetonitrile and 1.105 g (6 mmol) of Na($C_5H_4COCF_3$) was added. The reaction mixture was stirred for 12 h at room temperature during irradiation with simple 100 W visible-light lamp. Color gradually changed from orange to dark red. Solvents were removed in vacuum and waxy residue was extracted with boiling hexane (100 ml). After evaporation of hexane the residue was purified by column chromatography (Al_2O_3/hexane) giving dark red crystalline product (620 mg, 2.2 mmol, 73% yield). Recently reported synthesis describes **Tfa_1Fc** as cherry red liquid [28].

Mp 36–37 °C. UV–vis [hexane, λ_{max}, nm, €, log(M^{-1} cm^{-1})]: 471 (2.75), 385sh (2.67), 354 (2.99), 271 (3.75), 231 (4.00). ^{1}H NMR (C_6D_6, δ, ppm): 3.82 (s, 5H); 4.07 (s, 2H); 4.70 (s, 2H). ^{13}C NMR: 71.0 (s, Cp), 71.1 (q, $^4J_{CF}$ = 2.5 Hz, *C*H), 74.7 (s, *C*H), 117.9 (q, $^1J_{CF}$ = 295.2 Hz, *C*F_3), 186.2 (q, $^2J_{CF}$ = 36.6 Hz, *C*O), the signal of C_{ipso} was not detected; ^{19}F NMR: −72.0 (s, CF_3). IR (KBr pellet, cm^{-1}): 3116w (ν_{CH}), 1693vs (ν_{CO}), 1456m, 1414w, 1383w, 1321m, 1261m, 1219vs (ν_{CF}), 1186s (ν_{CF}), 1146vs, 1109m, 1057s, 1032m, 960m, 856m, 827m, 766m, 729m, 492m (δ_{FCF}). Raman (quartz capillary, cm^{-1}): 3111s (ν_{CH}), 3094m (ν_{CH}), 1690vs (ν_{CO}), 1214s (ν_{CF}), 1104vs ($\nu_{C=C}$, ring breathing of Cp), 1059m, 1030w, 762m, 728w, 604m (δ_{FCF}), 398m, 365w, 332s, 301s. Anal. Found: C, 50.86; H, 3.10%; $C_{12}H_9F_3FeO$ Calc.: C, 51.10; H, 3.22%.

2.6. Preparation of [Fe($C_5H_4COCF_3$)$_2$], Tfa_2fc

To a solution of 11.98 g Na($C_5H_4COCF_3$) (65 mmol) in 150 ml of THF 7.00 g $FeBr_2$ (32.5 mmol) was added at 0 °C. The mixture was stirred for 12 h at room temperature and for additional 2 h under reflux. Cooled mixture was poured into ice-cold water, organic layer was separated and residual suspension was extracted with 2 × 60 ml of CH_2Cl_2. Combined organic extracts were washed with brine until water layer remained yellow. Organic layer was dried with $MgSO_4$ and solvents were vacuum removed. Crude dark solid was chromatographed on Al_2O_3 using benzene as eluent. Red band containing product was collected, evaporated in vacuum and residue was crystallized from pentane at −60 °C giving 560 mg (1.5 mmol, 5% yield) of thin red needles.

Mp 56–57 °C. UV–vis [hexane, λ_{max}, nm, €, log(M^{-1} cm^{-1})]: 481 (2.77), 379sh (3.04), 351 (3.14), 264 (4.10), 228 (4.13). ^{1}H NMR (C_6D_6, δ, ppm): 3.97 (m, $^5J_{HF}$ = 2.0 Hz, 4H); 4.54 (s, 4H). ^{13}C NMR: 72.7 (s, *C*H), 76.4 (s, *C*H), 117.3 (q, $^1J_{CF}$ = 292.5 Hz, CF_3), 184.9 (q, $^2J_{CF}$ = 32.2 Hz, CO), the signal of C_{ipso} was not detected; ^{19}F NMR: −72.8 (s, CF_3). IR (KBr pellet, cm^{-1}): 3124w (ν_{CH}), 1701vs (ν_{CO}), 1458m, 1380m, 1323m, 1221vs (ν_{CF}), 1190s (ν_{CF}), 1148s (ν_{CF}), 1059m, 1035m, 962m, 858m, 770m, 731s, 486m (δ_{FCF}). Raman (quartz capillary, cm^{-1}): 3127m (ν_{CH}), 3118m (ν_{CH}), 3101w (ν_{CH}), 1700vs (ν_{CO}), 1459m, 1227m (ν_{CF}), 1055m, 766m, 731w, 604m (δ_{FCF}), 515w, 488w, 413m, 371m, 338s, 301s. Anal. Found: C, 44.32; H, 2.09%. $C_{14}H_8F_6FeO_2$ Calc.: C, 44.48; H, 2.13%.

3. Results and discussion

3.1. Surface hardness and drying time of the paint films

The drying activity of acyl-substituted ferrocenes was established on the solvent-borned phtalic type alkyd resin modified with tall oil. Fig. 1 shows hardness development of the film during the course of drying. Final relative hardness and drying time for each catalyst are listed in Table 1. The shortest drying times of 2.4 and 2.6 h were observed for monosubstituted derivatives **Bz_1Fc** and **Ac_1Fc**, respectively. These values are considerably lower than that obtained for commercial **Co Nuodex** drier. Disubstituted ferrocenes

Table 1
Autoxidation activity of studied compounds toward alkyd binder; concentration of drier was 0.1 wt.% of metal in solid dry matter.

Drier	$-k_{CH,\,max}$ (h^{-1}) [a]	t_{max} (h)[a]	IT (h)[b]	t_{conj} (h)[c]	τ (h)[d]	H_{rel} (%)[e]
Co Nuodex	0.82	0.48	0	2.2	8.6	50.2
Bz_1Fc	0.46	0.38	0	6.5	2.4	42.1
Ac_1Fc	0.33	0.57	0	8.5	2.6	39.6
Tfa_2fc	0.30	3.54	0.48	7.4	6.5	43.9
Tfa_1Fc	0.16	7.26	2.39	15.0	10.8	45.1
Bz_2fc	0.11	9.17	–[f]	18.0	16.2	45.8
Ac_2fc	0.13	16.62	7.65	22.9	20.2	43.0
Fc	0.04	~50	–[f]	~59	79.9	35.4
Alkyd	0.04	~50	–[f]	~63	82.0	34.4

[a] Maximum oxidation rate constant ($k_{CH,\,max}$) observed at drying time t_{max}.
[b] Induction time determined as the time period with k_{CH} less than 0.04 h^{-1}.
[c] Drying time in which the function shown in Fig. 5 has reached maximum.
[d] Drying times measured on a BYK drying recorder at 23 °C.
[e] Relative hardness of the film after 100 days.
[f] Not determined.

Bz_2fc and **Ac_2fc** are less effective but even they reduce the drying time of alkyd binder to approximately one-third. The lower drying activity of disubstituted acylferrocenes is probably due to quasi-reversible electrochemical behavior reported for **Ac_2fc** and **Bz_2fc**, respectively. [29,30] The sharp rise in relative hardness induced by acylferrocene derivatives at the start of the drying process is very promising feature due to reduction of film tackiness shortly after application of alkyd paint onto substrate, see Fig. 1. Unsubstituted ferrocene (**Fc**) has been examined for the purpose of comparison but its activity toward alkyd resin autoxidation is negligible.

3.2. FTIR analysis of alkyd autoxidation

The surface hardness measurements have shown that studied acyl-substituted ferrocenes are effective driers for alkyd resins but their role in the mechanism of autoxidation seems to be different from cobalt-based drier. IR spectroscopy has shown to be very useful tool for study the kinetics of oxidation of various systems containing fatty acids and their derivatives [31]. The autoxidation of alkyd resin catalyzed by acylferrocenes was studied by standard transmission technique. IR spectra of alkyd resin containing drier were measured immediately after application onto NaCl crystal and compared with that recorded after few hours. The main differences between these spectra were observed in regions ~3500, ~3008 and ~1000 cm^{-1}.

Broad intense band at ~3500 cm^{-1} was assigned to OH stretching of hydroxyl-containing species in binder system such as alkyd oxidation products (hydroperoxides, alcohols, water, etc.) or carboxylic functions originating from incomplete esterification of phthalic andydride. Sharp band at 3008 cm^{-1} was assigned to the antisymmetric CH stretching of allylic methylene group. Set of bands in region 1011–947 cm^{-1} is associated with vibrations of the *cis–trans* and *trans–trans* conjugated double bonds.

The monitoring of the integral intensity of the band at 3008 cm^{-1} with the time follows the abstraction of methylenic hydrogen from substrate [5]. The logarithmic plot of integrated area *vs* drying time yields a straight line for liquid model compounds such as ethyllinoleate indicating pseudo-first-order behavior of the autoxidation. This method is routinely used for the evaluation of drier activity in the autoxidation of unsaturated systems [8]. Although the alkyd resin shows different behavior during the drying process due to diffusional limitations in the hardening paint film, analysis of this peak area gives useful information about the rate of the alkyd autoxidation and the shape of obtained curve is closely related to the activity of the used drier [5]. The Fig. 2 shows logarithmic plots of peak area at 3008 cm^{-1} for studied driers. The estimated maximum rate constants $k_{CH,\,max}$ are listed in Table 2. The most powerful drier is commercial **Co Nuodex** having the steepest slope yielding a rate constant of 0.82 h^{-1} after 29 min of drying. Derivatives **Bz_1Fc** and **Ac_1Fc** also exhibit good drying activity with oxidation rate constant of 0.46 h^{-1} and 0.34 h^{-1} after 23 and 34 min, respectively. Other studied ferrocene derivatives are less effective showing maximum rate constants 0.3–0.1 h^{-1}, in time t_{max} 200–1000 min. Additionally, ferrocenes **Tfa_2fc**, **Tfa_1Fc**

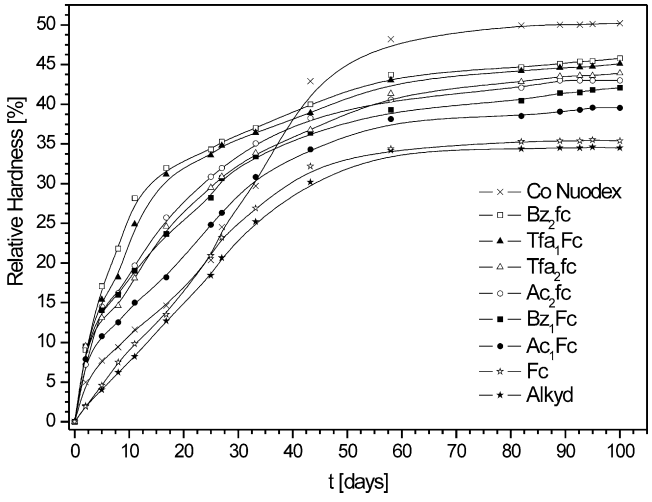

Fig. 1. Relative hardness of paint film during the course of drying with studied compounds.

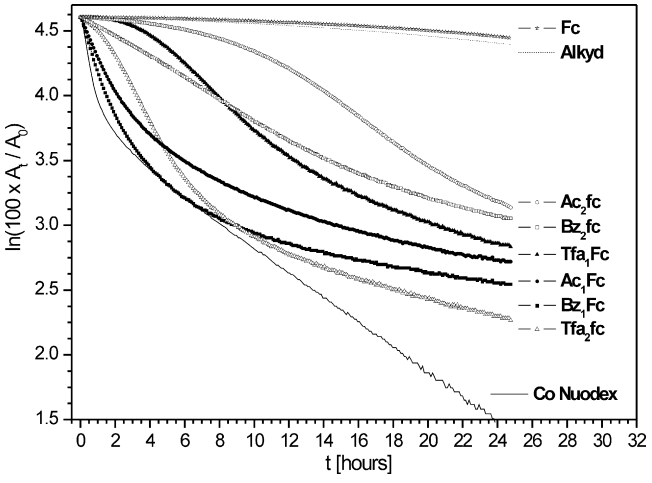

Fig. 2. Time dependent integral plots of the 3008 cm^{-1} band observed in alkyd autoxidation catalyzed with studied ferrocenes, **Co Nuodex** and pure alkyd. A_0 is area of the peak at the start of the measurement and A_t is actual peak area.

Table 2
Drying time (τ) and relative hardness (H_{rel}) for alkyd films dried with various mixtures of acylferrocene and **Co Nuodex**.

Concentration of metal		Used acylferrocene							
Co (%)	**Fe** (%)	**Bz_1Fc**		**Ac_1Fc**		**Bz_2fc**		**Ac_2fc**	
		τ (h)	H_{rel} (%)	τ (h)	H_{rel} (%)	τ (h)	H_{rel} (%)	τ (h)	H_{rel} (%)
0.010	0.065	1.1	55.8	6.0	53.9	14.0	53.7	17.9	54.4
0.015	0.060	0.8	55.1	3.0	56.8	6.8	56.5	8.6	56.1
0.020	0.055	0.8	48.9	3.0	47.0	7.0	49.3	7.5	47.5
0.025	0.050	0.6	51.7	3.0	51.8	3.5	49.3	7.3	50.5
0.050	0.025	1.0	55.1	2.0	55.1	2.8	55.9	3.0	56.1
0.025	0.025	0.9	55.8	2.5	55.6	4.3	55.9	6.8	56.3

and **Ac_2fc** exhibit noticeable induction period during which the radical reaction does not proceed and the rate constant is less than maximum one observed in drying of pure alkyd resin ($k_{CH,\,max}$ is 0.04 h^{-1}). Parent complex, **Fc**, slightly slows down the rate of methylenic hydrogen abstraction and its effect in autoxidation process could be described as inhibitive.

Fig. 3 shows the changes of IR spectra in the region of OH stretching during the course of drying. At the start of the oxidation process, the maximum of this band is localized at 3523 cm^{-1} corresponding to ν_{OH} of carboxylic function [32]. As the oxidation of alkyd proceeds, the shape of the band changes. After 5 h, the local maximum was observed at 3446 cm^{-1}. The band rises in intensity due to forming of oxidation products such as hydroperoxides or alcohols produced by their subsequent decomposition. Integrated area in the region 3650–3125 cm^{-1} was found to be markedly temperature dependent, when band area decreases with increasing temperature. This observation indicates significant contribution of thermally labile hydroperoxide ν_{OH} stretching to the overall intensity of this band. Rising of band intensity during the drying of alkyd resin thus reflects the formation hydroperoxides and their decomposition products (alcohols and carboxylic acids); see Fig. 4. In pure alkyd, the concentration of OH-containing species quickly increases in the first 40 min as hydroperoxides are formed. In the absence of drier, hydroperoxides are only slowly decayed and further growth of OH-containing species is slow. All studied acylferrocenes decompose hydroperoxides into OH-containing products resulting in successive increase of the band intensity. **Co Nuodex** showed the highest drying activity having the steepest curve, followed with less active ferrocenes **Bz_1Fc** and **Ac_1Fc**, respectively. Low active complexes **Tfa_1Fc** and **Ac_2fc** exhibit deflected shape of the curve probably due to induction period observed in these systems.

Completely different behavior showed **Fc**, which decreases the concentration of OH–containing species in the course of drying, as could be seen from the Fig. 4. If we assume that **Fc** is able to decay hydroperoxides, resulting radicals seems be consumed in reactions different from those yielding new hydroperoxides. Thus propagation step in the system containing unsubstituted ferrocene is hindered. Inhibitive effect is probably due to reaction of stable ferrocenium cation with present radicals giving ring-substituted derivatives:

$$[Fe(\eta^5\text{-}C_5H_5)_2]^+ + R^\bullet \rightarrow [Fe(\eta^5\text{-}C_5H_4R)(\eta^5\text{-}C_5H_5)] + H^+$$

Ring-substituted ferrocenes bearing electron-releasing groups are poor driers [20,21] and the rate of alkyd autoxidation is further decreased. The radical reactions of stable ferrocenium salts have been described previously and they are rarely used for the preparation of some ring – substituted ferrocene derivatives [33]. Ring-substituted ferrocenium and particularly oxidized acylferrocenes do not react with radicals in this manner.

Hydrogen atom abstraction from methylenic CH group produces reactive carbon-centered radicals that, after fast reaction with oxygen, give hydroperoxides containing conjugated double bonds [8]. The vibrations of *cis–trans* and *trans–trans* conjugated double bonds are observable as medium bands in region 1011–947 cm^{-1} [6,34]. Fig. 5 depicts changes in the intensity of this band during the course of drying. Since the rearrangement of isolated double bonds to conjugated system is directly associated with the initiation of autoxidation process, rising intensity of this band during the autoxidation is expectable. After consuming of majority of methylene functions in the coating band intensity decreases as reactive conjugated double bonds react with present radicals. We can consider this point as the end of extensive alkyd oxidation when cross-linking saturation reactions prevail over the formation of radicals.

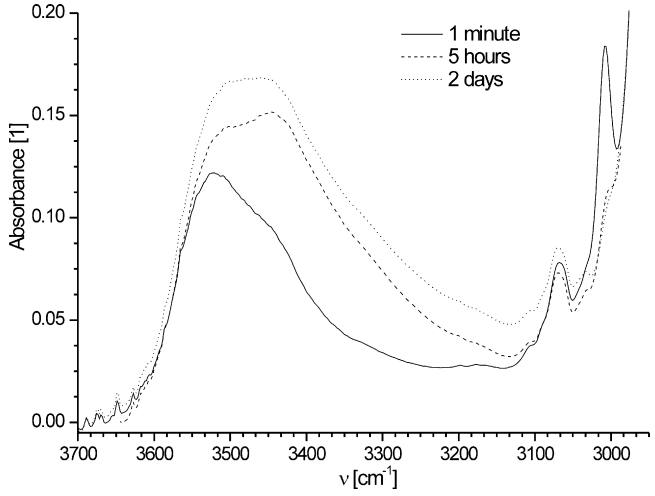

Fig. 3. Detailed view of FT-IR spectrum change during alkyd autoxidation in the region of OH stretching and methylenic CH stretching.

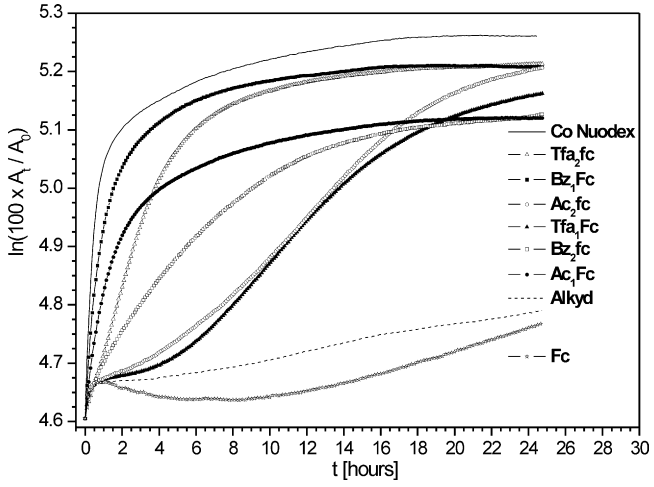

Fig. 4. Increase of OH containing species monitored by time-resolved FT-IR during the alkyd autoxidation.

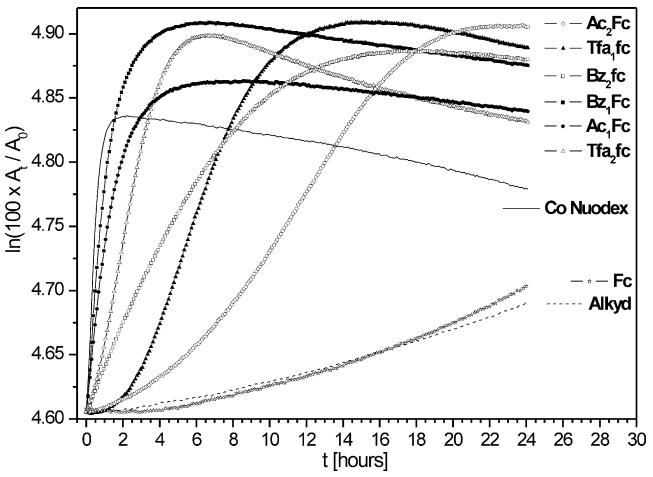

Fig. 5. Time dependent integral plots of bands corresponding to vibrations of conjugated double bonds.

The most potent driers **Co Nuodex** and **Bz$_1$Fc** have this time (t_{conj}) of 2.20 and 6.49 h, respectively. The curve for the least effective acylferrocene, **Ac$_2$fc**, reaches its maximum after 22.90 h. Further important information about the mechanism was obtained from the comparison of rate constant k_{CH} determined in the time t_{conj}. For all studied acylferrocenes, this constant varies in narrow range 0.06–0.07 h^{-1}. Only **Co Nuodex** has k_{CH} of 0.25 h^{-1} in time t_{conj}. It indicates that the saturation reactions are faster in the alkyd binder dried with **Co Nuodex** than in acylferrocene-catalyzed systems. The compound **Fc** expectedly shown the lowest growth in the concentration of conjugated double bonds.

3.3. Synergic effect between acylferrocenes and cobalt-based drier

The applicability of acylferrocenes in the alkyd paint formulations was further examined on the mixed drier systems based on acylferrocene and **Co Nuodex** at lower metal content in the solid film (0.075 and 0.05 wt.%). This part covers only commercially available ferrocene derivatives **Ac$_1$Fc**, **Bz$_1$Fc**, **Ac$_2$fc** and **Bz$_2$fc**. Drying times and final hardness of the prepared alkyd films containing various amount of acylferrocenes and cobalt-based drier are summarized in Table 2.

These data prove that all studied acylferrocenes exhibit synergic effect when used in mixture with Co(II) drier. The best results were obtained for **Bz$_1$Fc** – **Co Nuodex** system giving in whole concentration range shorter drying times (0.6–1.1 h) than both pure **Bz$_1$Fc** and **Co Nuodex**, respectively (*cf.* Table 1). This system enables to reduce cobalt content to 0.01 wt.% (with Fe content 0.065 wt.%). Final hardness of the prepared film then exceeds that obtained for **Co Nuodex** (0.1 wt.%) by 10%. Significant shortening of the drying time and the increase of film hardness has been observed also for the systems containing **Ac$_1$Fc**, **Ac$_2$fc** and **Bz$_2$fc**. In these case the optimal concentrations of Co(II) and Fe(II) are 0.05 and 0.025, respectively.

Monoacylferrocenes **Ac$_1$Fc** and **Bz$_1$Fc** show at concentration 0.025 wt.% only low drying activity with $k_{CH,\,max}$ of 0.12–0.13 h^{-1}, see Table 3. Diacylferrocenes are not active as driers at this concentration. The obtained kinetic data indicate rather inhibiting activity of **Ac$_2$fc** and **Bz$_2$fc**, respectively. Oxidation rate constants for **Ac$_2$fc** and **Bz$_2$fc** were lower than that observed for pure alkyd resin within 5 days of drying. **Co Nuodex** at concentration 0.025 wt.% has activity comparable to 0.1 wt.% of **Ac$_1$Fc** or **Tfa$_2$Fc** (*cf.* Table 3). The most remarkable feature is the appearance inhibition period in this system. Addition of studied acylferrocenes (0.025 wt.%) to alkyd composition containing 0.025% of **Co Nuodex** significantly enhances the activity of drying system as could be seen from kinetic data listed in Table 3. Maximum oxidation rate constant $k_{CH,\,max}$ in the mixed systems vary between 0.35 h^{-1} and 0.42 h^{-1} and t_{max} and t_{conj} are considerably shorter. Significant shortening of inhibition time (0–1.67 h) is also apparent.

3.4. Autoxidation of model compounds by ferrocene derivatives

For the determination of drying activity of various compounds model systems such as e.g. methyloleate, methyl ricinoate, ethyllinoleate (EL) or methyl linolenate (ML) are routinely used [7,31]. It is surprising that time dependent FTIR measurements of EL autoxidation catalyzed by ferrocene driers showed no or negligible activity with the rate constants k_{CH} less than 10^{-3} h^{-1}. **Co Nuodex** has corresponding constant of 0.26 h^{-1} under identical conditions (Ref. [5] reports 0.24 h^{-1}). The differences in catalytic activity of various driers for alkyd and EL have been described previously but were not yet satisfactorily explained [5]. We found that the addition of small amount of carboxylic acids, such as 2-ethylhexanoic acid (EHA), phthalic acid or trifluoroacetic acid, to the model system leads to significant increasing of autoxidation rate constant. Maximum rate constant of 0.12 h^{-1} for **Bz$_1$Fc** (0.1% Fe in dry alkyd) was observed at EHA-to-drier molar ratio 1:1. It suggests that carboxylic acid reacts with drier enhancing its activity toward EL oxidation. Thus one factor contributing to faster autoxidation of alkyd resins by ferrocene derivatives could be the presence of free carboxylic groups originating from incomplete esterificaton of phthalic anhydride. Carboxylic acid reacts with hydroxyl anion produced during the oxidation of drier. Resulting carboxylate anion also could stabilize oxidized form of drier by compensating its positive charge:

$$R'COOH + ROOH + Fc \rightarrow RO^{\bullet} + Fc^{+} + R'COO^{-} + H_2O$$

These results are fully in agreement with the increasing rate of linoleic acid hydroperoxide decomposition at lower pH catalyzed by ferrous ion or by ferrocene monocarboxylic acid, respectively [19]. Formation of ferrocenium cation seems be the key step in the mechanism of autoxidation process. Unfortunately, fast reaction of hydroperoxides with ferrocenes in acidic aqueous solutions disables simple determination of peroxide value in these systems using standard analytical methods, such as oxidation iodide to triiodide or the reaction with thiobarbituric acid [19,35].

We have tried to examine autoxidation of linoleic (LA) and linolenic acid (LnA) catalyzed by ferrocene driers but we find out that these acids are not suitable as a model compounds for time-resolved FTIR study. Both acids are readily skimmed with waxy crust on the surface of sample spread on ATR crystal and measured spectra are only poorly reproducible. Moreover, fatty acids cannot be used as model systems also owing to low solubility of studied ferrocenes in them disabling the preparation of samples with metal content higher than 0.05 wt.%.

3.5. ESR study of t-butylhydroperoxide decomposition

As we mentioned above, the most important function of drier is the reaction with relatively stable hydroperoxides giving alkoxy and peroxy radicals. Hence, we investigated decomposition of *t*-butylhydroperoxide by studied ferrocenes, ferrocenium tetrafluoroborate (**FcBF$_4$**) and **Co Nuodex** in the presence of various spin traps. All experiments were performed in the presence of air atmosphere resembling to real conditions in the course of alkyd drying. Although all studied ferrocene derivatives including unsubstituted ferrocene (**Fc**) gave identical ESR spectra during our experiments, the benzoyl derivative **Bz$_1$Fc** was chosen because it has shown the shortest induction period and the highest concentration of

Table 3
Kinetic data of alkyd films used for FTIR examination of synergic effects.

Concentration of metal		Acylferrocene	$-k_{CH,\,max}$ (h^{-1}) [a]	t_{max} (h)[a]	IT (h)[b]	t_{conj} (h)[c]	τ (h)
Co (%)	**Fe** (%)						
–	0.025	**Bz_1Fc**	0.13	4.51	0.29	13.9	14.3
–	0.025	**Ac_1Fc**	0.12	5.72	0.32	14.7	13.8
–	0.025	**Bz_2fc**	[d]	[e]	[e]	[e]	37.3
–	0.025	**Ac_2fc**	[d]	[e]	[e]	[e]	50.4
0.025	0.025	**Bz_1Fc**	0.42	2.41	0	4.4	0.9
0.025	0.025	**Ac_1Fc**	0.37	2.50	0.10	4.6	2.5
0.025	0.025	**Bz_2fc**	0.41	5.14	0.85	6.7	4.3
0.025	0.025	**Ac_2fc**	0.35	5.80	1.67	7.8	6.8
0.025	–	–	0.31	9.61	4.36	11.6	7.4

[a] Maximum oxidation rate constant ($k_{CH,\,max}$) observed at drying time t_{max}.
[b] Induction time determined as the time period with k_{CH} less than 0.04 h^{-1}.
[c] Drying time in which the concentration of conjugated double-bonds has reached maximum.
[d] Less than 0.04 h^{-1}.
[e] Not determined.

generated radical species. Ferrocenium salt **$FcBF_4$** has been involved to our study to assess our hypothesis that hydroperoxides are cleaved quickly by oxidized ferrocene derivatives. Pure oxidized congeners of acylferrocenes were not used due to instability of corresponding ferrocenium salts [36].

Since radicals such as ROO•, RO• and R• have very short half-life, standard ESR technique cannot detect them without the use of some spin-trapping methods. Commonly used spin traps are nitrone derivatives such as α-phenyl-N-*t*-butylnitrone (PBN) or 5,5-dimethyl-1-pyrroline *N*-oxide (DMPO) [37]. Scheme 2 shows structures of spin traps used in this study for the distinguishing between ROO•, RO• radicals.

Spin trap DMPO is not suitable for this study due to fast decomposition of peroxoradical adduct ^{t}BuOO•/DMPO resulting in solely observation of alkoxy radical adducts ^{t}BuO•/DMPO and MeO•/DMPO in our systems [38]. Spin trap PBN is better for distinguishing peroxy radicals from alkoxy radicals than DMPO but major drawback of this spin trap is short lifetime of its oxygen-centered radical adducts [39]. This fact somewhat complicates recording of well-resolved ESR spectra suitable for computer simulation analysis because quality continuous wave ESR spectra are usually recorded within 6 min (see Section 2.3). Moreover, peroxy and alkoxy radicals give spin adducts with similar hyperfine coupling constants and resolving of ^{t}BuO•/PBN and ^{t}BuOO•/PBN species in the mixture requires higher concentration of radicals in the sample [40,41].

Fig. 6 shows ESR spectra of PBN adducts generated during the decomposition of ^{t}BuOOH by **Bz_1Fc**, **$FcBF_4$** and **Co Nuodex**, respectively. Ferrocene derivatives slowly generate low concentration of alkoxy radicals after mixing with hydroperoxide. When ferrocenium salt **$FcBF_4$** was used, two species were immediately detected. The strongest signal (a_N = 1.32 mT, a_H = 0.13 mT, 79% area) was assigned to ^{t}BuOO•/PBN and 3-line signal with a_N = 0.79 mT is oxidized spin trap, benzoyl *tert*-butyl nitroxide (PBNX) [42]. **Co Nuodex** decomposes ^{t}BuOOH giving ESR spectrum corresponding to the mixture of ^{t}BuOO•/PBN, ^{t}BuO•/PBN and PBNX species in the area ratio 5:2:3. The obtained spectrum is very close to that previously reported in the ESR study of ^{t}BuOOH decomposition by $Co(acac)_2$ in degassed benzene solutions [43]. Reactions giving observed radicals are as follows:

$$FcBF_4 + {}^tBuOOH \rightarrow Fc + HBF_4 + {}^tBuOO^{\bullet}\ (\text{very fast})$$

$$Fc + {}^tBuOOH \rightarrow Fc^+ + OH^- + {}^tBuO^{\bullet}\ (\text{slow})$$

In 1983 Niki et al. reported that methyl-*N*-duryl nitrone (MDN) successively traps oxygen-centered radicals ROO• and RO• [43,44]. Spin adducts observed were clearly distinguished owing to sufficiently different hyperfine splitting constants, see Table 4. Unfortunately, synthesis of analytically pure MDN has not been published to date and generally known low-yield multistep procedures utilize relatively expensive materials. Based on close structural similarity (see Scheme 2) to MDN, we have used methyl-*N*-mesityl nitrone (MMN) as a spin trap in our study. MDN and MMN species have identical environment in the neighborhood of nitrone group and thus similar ESR coupling constants of their radical adducts are expectable. For the preparation of MMN simple UV photolysis of commercially available nitromesitylene has been used [26].

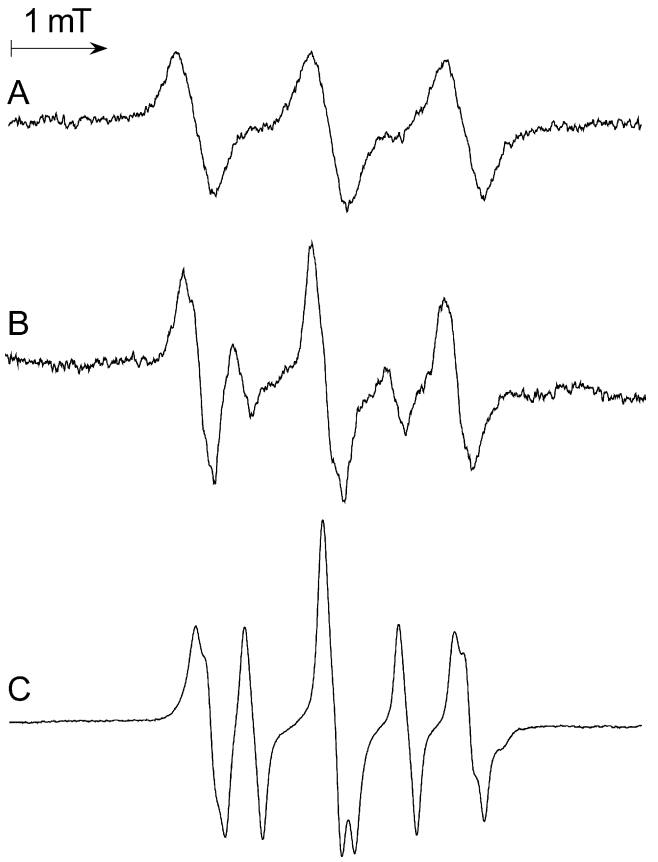

Fig. 6. ESR spectra of observed PBN spin adducts in toluene solution. (A) **Bz_1Fc** after 130 min, (B) **$FcBF_4$** after 6 min, (C) **Co Nuodex** after 6 min. For experimental details see Section 2.3.

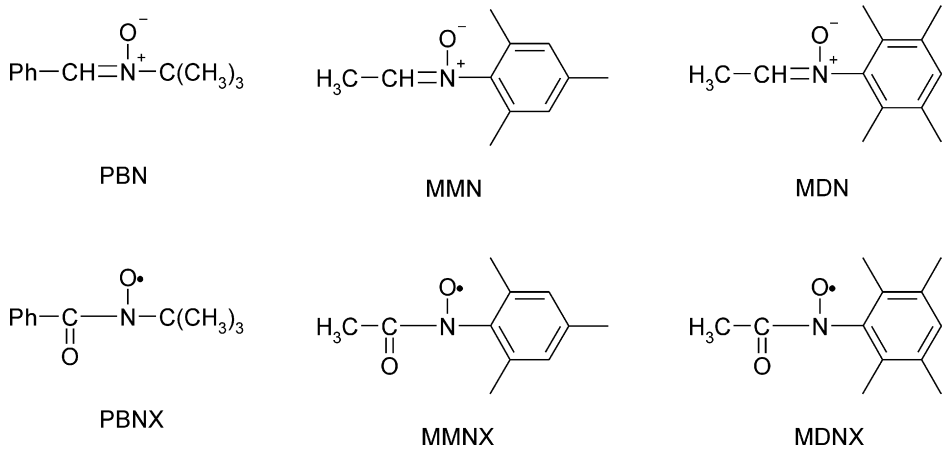

Scheme 2. Spin-traps (top) and oxidized spin-trap radicals (bottom) mentioned in the text.

Observed hyperfine-splitting constants of MMN spin adducts listed in Table 4 are very close to that reported for MDN. This spin trap was found to be suitable for distinguishing of peroxy and alkoxy radicals. From the Fig. 7 it is clearly seen that ferrocene derivative generates primarily alkoxy radical from ^{t}BuOOH in toluene whereas ferrocenium salt gives ^{t}BuOO•/MMN adduct under identical conditions. Since spin adducts of nitrones with peroxy radicals are unstable at ambient conditions, signal of ^{t}BuOO•/MMN was accompanied with triplet signal (6% of area) of MMN oxidized form, acetyl-*N*-mesitylnitroxide (MMNX), analogously to PBN and MDN spin traps. Mechanism of this oxidation has been proposed previously [43,45].

The use of MMN spin trap enables to identify three radical species generated by the decomposition of ^{t}BuOOH by **Co Nuodex** in toluene, the most intense being peroxy radical adduct. Area percentage ratio of ^{t}BuOO•/MMN, ^{t}BuO•/MMN and MMNX signals was found to be 5:3:2. Different ratio of MMN adducts in the mixture compared to PBN probably reflects different rate constants for spin scavenging of radicals and radical adduct decomposition, respectively. After exposition of the mixture to diffuse light for 120 min, solely three-line ESR signal of oxidized spin trap species MMNX was observed.

The ESR study has shown that ferrocene derivatives slowly decompose ^{t}BuOOH to give alkoxy radicals after some induction period. Peroxy radicals were not observed in this system due to short life-time of peroxy radical adducts with used spin traps. Ferrocenium compound immediately generates peroxy radicals that, after scavenging by PBN and MMN, subsequently yield radical species of oxidized spin trap PBNX and MMNX, respectively. The fastness of reaction between **$FcBF_4$** and ^{t}BuOOH is also evident from the change in the color of the mixture. Characteristic blue–green solution of ferrocenium salt instantly fades to give yellow color of reduced ferrocene after the addition of ^{t}BuOOH.

Table 4
ESR hyperfine splitting constants for spin trap adducts.

Radical species	Observed values		Reference values	
	a_N (mT)	a_H (mT)	a_N (mT)	a_H (mT)
^{t}BuO•/PBN	1.39	0.19	1.41[a]	0.18[a]
^{t}BuOO•/PBN	1.32	0.13	1.34[a]	0.14[a]
PBNX	0.79	–	0.80[a]	–
^{t}BuO•/MMN	1.35	0.71	1.41[b]	0.75[b]
^{t}BuOO•/MMN	1.24	0.41	1.28[b]	0.46[b]
MMNX	0.71	–	0.73[c]	–

[a] PBN adducts and PBNX radical [40].
[b] MDN adducts [44].
[c] MDNX radical [44].

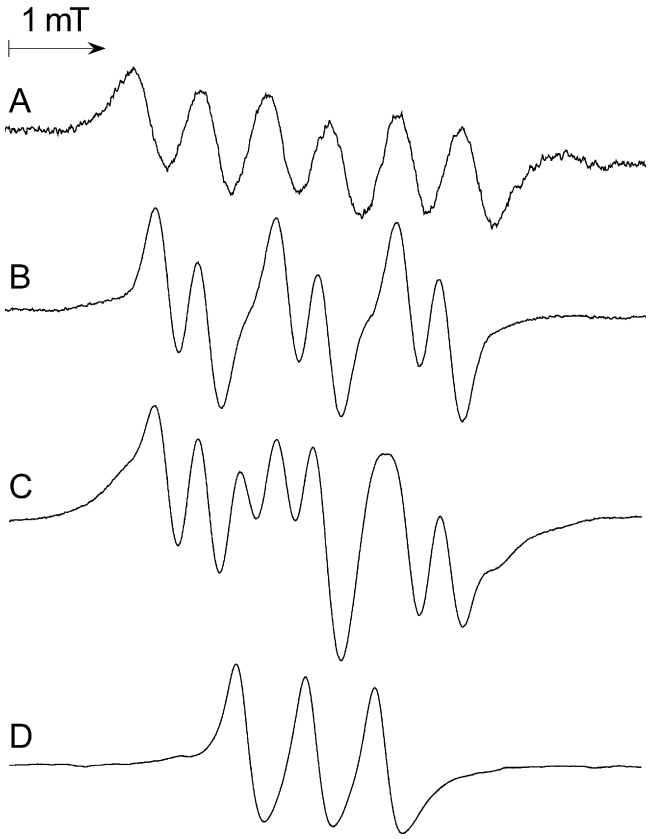

Fig. 7. ESR spectra of spin adducts observed during the decomposition of ^{t}BuOOH by studied driers in the presence of MMN. (A) **Bz_1Fc** after 130 min, (B) **$FcBF_4$** after 6 min, (C) **Co Nuodex** after 6 min, (D) **Co Nuodex** after 120 min exposition to laboratory light. For experimental details see Section 2.3.

4. Conclusions

This study has shown that acyl-substituted ferrocenes are active driers for solvent-borne alkyd paints. Drying times observed for derivatives **Ac_1Fc** and **Bz_1Fc** are shorter than that observed for commercial **Co Nuodex**. Disubstituted ferrocene derivatives showed lower efficiency. Much longer drying time observed for highly active cobalt(II) drier could be explained by fast polymerization on the top surface of the coating film while the inner bulk remains plastic and soft. Acyl-substituted ferrocenes showed also advantage in rising of the film hardness at the start of the drying process. They reduce stickiness of alkyd film after application onto substrate. Final

hardness of polymer films dried by studied ferrocene derivatives is slightly lower than that for **Co Nuodex** probably due to lower concentration of radicals in the composition or due to different nature of present radicals. FTIR study of alkyd autoxidation kinetics confirmed different behavior of ferrocene driers and **Co Nuodex**, respectively. Kinetic data obtained from time-dependent FTIR measurements could be used for the determination of drier activity toward alkyd autoxidation. Unsubstituted ferrocene surprisingly showed inhibiting activity toward alkyd autooxidation. This observation could be explained on the basis of radical reaction with ferrocenium cation giving substituted ferrocene. Acylferrocenes show an excellent synergic effect with **Co Nuodex**, giving polymeric films with physical properties better than those observed for pure driers. Addition of small amount of acylferrocene into alkyd composition enables significant reduction of Co(II) content in the composition. Synergic effects in the mixed drier systems were also confirmed by kinetic FTIR measurements.

Low catalytic activity of acylferrocenes toward autoxidation of model compounds such as EL or ML is significantly enhanced in the presence of carboxylic acid. This acceleration is probably caused by easier oxidation of acylferrocene drier in acidic media, which is responsible for subsequent decomposition of hydroperoxides yielding highly reactive peroxoradical species.

The ESR study proved that ferrocenes and cobalt-based drier decompose hydroperoxides giving different radicals. Ferrocene and its acylderivatives slowly react with hydroperoxides yielding alkoxy radicals, whereas cobalt-based drier affords a mixture of alkoxy and peroxy radicals. Ferrocenium salt instantaneously cleaves hydroperoxide to give peroxy radicals. Thus in the composition dried with ferrocene derivatives, the major amount of drier occurs in its reduced form. By contrast, cobalt-based driers are present as a mixture of Co(II) and Co(III) species. For the distinguishing between peroxy and alkoxy radicals, the new spin trap MMN was used.

Acknowledgements

Financial supports from Czech Science Foundation (grant GA 104/09/0529) and from the Ministry of Education, Youth and Sports of the Czech Republic (research project MSM 0021627501) are gratefully acknowledged.

References

[1] S. Friebel, O. Deppe, Chem. Ing. Tech. 80 (2009) 1721–1752.
[2] F.S. Guner, Y. Yagci, A.T. Erciyes, Prog. Polym. Sci. 31 (2006) 633–670.
[3] N.A. Porter, S.E. Caldwell, K.A. Mills, Lipids 30 (1995) 277–290.
[4] J.H. Bieleman, Macromol. Symp. 187 (2002) 811–822.
[5] W.J. Muizebelt, J.C. Hubert, M.W.F. Nielen, R.P. Klaasen, K.H. Zabel, Prog. Org. Coat. 40 (2000) 121–130.
[6] J. Mallegol, J. Lemaire, J.L. Gardette, Prog. Org. Coat. 39 (2000) 107–113.
[7] Z.O. Oyman, W. Ming, R. van der Linde, Prog. Org. Coat. 48 (2003) 80–91.
[8] R. van Gorkum, E. Bouwman, Coord. Chem. Rev. 249 (2005) 1709–1728.
[9] D. Lison, M. De Boeck, V. Verougstraete, M. Kirsch-Volders, Occup. Environ. Med. 58 (2001) 619–625.
[10] J.R. Bucher, J.R. Hailey, J.R. Roycroft, J.K. Haseman, R.C. Sills, S.L. Grumbein, P.W. Mellick, B.J. Chou, Toxicol. Sci. 49 (1999) 56–67.
[11] M. De Boeck, M. Kirsch-Volders, D. Lison, Mutat. Res.: Fundam. Mol. M 548 (2004) 127–128.
[12] J.Z. Wu, E. Bouwman, J. Reedijk, Prog. Org. Coat. 49 (2004) 103–108.
[13] R. van Gorkum, E. Bouwman, J. Reedijk, Inorg. Chem. 43 (2004) 2456–2458.
[14] N.G. Connelly, W.E. Geiger, Chem. Rev. 96 (1996) 877–910.
[15] E. Antolini, E.R. Gonzalez, Appl. Catal. A: Gen. 365 (2009) 1–19.
[16] F. Chen, N.J. Tao, Acc. Chem. Res. 42 (2009) 429–438.
[17] N. Chavain, C. Biot, Curr. Med. Chem. 17 (2010) 2729–2745.
[18] J.B. Shi, C.J.W. Jim, F. Mahtab, J.Z. Liu, J.W.Y. Lam, H.H.Y. Sung, I.D. Williams, Y.P. Dong, B.Z. Tang, Macromolecules 43 (2010) 680–690.
[19] A. Mulchandani, D.C. Rudolph, Anal. Biochem. 225 (1995) 277–282.
[20] P. Kalenda, J. Holeček, D. Veselý, M. Erben, Prog. Org. Coat. 56 (2006) 111–113.
[21] V. Štáva, M. Erben, D. Veselý, P. Kalenda, J. Phys. Chem. Solids 68 (2007) 799–802.
[22] M. Erben, Z. Padělková, P. Štěpnička, D. Veselý, M. Dušek, Inorg. Chim. Acta 363 (2010) 3365–3375.
[23] P. Kalenda, D. Veselý, A. Kalendová, V. Šťáva, Pigm. Resin Technol. 39 (2010) 342–347.
[24] D.J. Burkey, M.L. Hays, R.E. Duderstadt, T.P. Hanusa, Organometallics 16 (1997) 1465–1475.
[25] A.K. Diallo, J. Ruiz, D. Astruc, Inorg. Chem. 49 (2010) 1913–1920.
[26] D. Döpp, D. Muller, Recl. Trav. Chim. Pays-Bas 98 (1979) 297–302.
[27] S. Barry, A. Kucht, H. Kucht, M.D. Rausch, J. Organomet. Chem. 489 (1995) 195–199.
[28] M. Sobočíková, P. Štěpnička, D. Ramella, M. Kotora, Collect. Czech. Chem. Commun. 71 (2006) 190–196.
[29] D. Osella, A. Carretta, C. Nervi, M. Ravera, R. Gobetto, Organometallics 19 (2000) 2791–2797.
[30] H. Choi, J.W. Hershberger, A.R. Pinhas, D.M. Ho, Organometallics 10 (1991) 2930–2936.
[31] S.T. Warzeska, M. Zonneveld, R. van Gorkum, W.J. Muizebelt, E. Bouwman, J. Reedijk, Prog. Org. Coat. 44 (2002) 243–248.
[32] D. Peltier, A. Pichevin, Bull. Soc. Chim. Fr. (1960) 1141–1147.
[33] A.L. Beckwith, R.J. Leydron, Tetrahedron 20 (1964) 791–801.
[34] J.H. Hartshorn, J. Coat. Technol. 54 (1982) 53–61.
[35] G.W. Kurtz, E.F. Price, S. Patton, J. Dairy Sci. 34 (1951), 484-484.
[36] P. Carty, M.F.A. Dove, J. Organomet. Chem. 28 (1971) 125–132.
[37] G.R. Buettner, Free Radical Biol. Med. 3 (1987) 259–303.
[38] C.M. Jones, M.J. Burkitt, J. Chem. Soc., Perkin Trans. 2 (2002) 2044–2051.
[39] E.G. Janzen, Y. Kotake, R.D. Hinton, Free Radical Biol. Med. 12 (1992) 169–173.
[40] D.L. Haire, U.M. Oehler, P.H. Krygsman, E.G. Janzen, J. Org. Chem. 53 (1988) 4535–4542.
[41] A. Ledwith, P.J. Russell, L.H. Sutcliffe, Proc. R. Soc. London A 332 (1973) 151–166.
[42] S.V. Verstraeten, S. Lucangioli, M. Galleano, Inorg. Chim. Acta 362 (2009) 2305–2310.
[43] E. Niki, S. Yokoi, J. Tsuchiya, Y. Kamiya, J. Am. Chem. Soc. 105 (1983) 1498–1503.
[44] T. Yamada, E. Niki, S. Yokoi, J. Tsuchiya, Y. Yamamoto, Y. Kamiya, Chem. Phys. Lipids 36 (1984) 189–196.
[45] M.V. Merritt, R.A. Johnson, J. Am. Chem. Soc. 99 (1977) 3713–3719.